Research Article

Journal of Physical Organic Chemistry

Received: 11 May 2008, Revised: 19 June 2008, Accepted: 20 June 2008, Published online in Wiley InterScience: 21 July 2008

(www.interscience.wiley.com) DOI 10.1002/poc.1424

Two-phase flow electrosynthesis: Comparing *N*-octyl-2-pyrrolidone–aqueous and acetonitrile–aqueous three-phase boundary reactions

Stuart M. MacDonald[a], John D. Watkins[a], Stephen D. Bull[a], Iwan R. Davies[a], Yunfeng Gu[b], Kamran Yunus[b], Adrian C. Fisher[b], Philip C. Bulman Page[c], Yohan Chan[c], Claire Elliott[d] and Frank Marken[a]*

A microfluidic double channel device is employed to study reactions at flowing liquid–liquid junctions in contact with a boron-doped diamond (BDD) working electrode. The rectangular flow cell is calibrated for both single-phase liquid flow and biphasic liquid–liquid flow for the case of (i) the immiscible *N*-octyl-2-pyrrolidone (NOP)–aqueous electrolyte system and (ii) the immiscible acetonitrile–aqueous electrolyte system. The influence of flow speed and liquid viscosity on the position of the phase boundary and mass transport-controlled limiting currents are examined. In contrast to the NOP–aqueous electrolyte case, the acetonitrile–aqueous electrolyte system is shown to behave close to ideal without 'undercutting' of the organic phase under the aqueous phase. The limiting current for three-phase boundary reactions is only weakly dependent on flow rate but directly proportional to the concentration and the diffusion coefficient in the organic phase. Acetonitrile as a commonly employed synthetic solvent is shown here to allow effective three-phase boundary processes to occur due to a lower viscosity enabling faster diffusion. *N*-butylferrocene is shown to be oxidised at the acetonitrile–aqueous electrolyte interface about 12 times faster when compared with the same process at the NOP–aqueous electrolyte interface. Conditions suitable for clean two-phase electrosynthetic processes without intentionally added supporting electrolyte in the organic phase are proposed. Copyright © 2008 John Wiley & Sons, Ltd.

Keywords: phase transfer catalysis; electrochemistry; microfluidic; phase boundary; ion extraction; electrosynthesis; ion transfer; voltammetry; green chemistry

INTRODUCTION

Electrosynthesis in microfluidic reactors[1–4] is a challenging but potentially highly beneficial approach to clean synthetic technology[5] in particular in combination with robotic combinatorial synthesis processes.[6,7] One objective in flow electrochemistry is the minimisation of waste and the elimination of intentionally added electrolyte that causes separation problems and product contamination issues.[8] Over the recent years, there have been several attempts to minimise supporting electrolyte in electrosynthesis based on (i) easily separated solid support systems,[9,10] (ii) small gap reactors in which the reactants and reaction intermediates provide sufficient conductivity[11,12] and (iii) two-phase flow microfluidic systems in which the reagent flow and the supporting electrolyte flow are kept separate.[13,14] The latter approach could be very effective for a range of standard chemical transformations including oxidations, epoxidations, ozonolyses, halogenation processes, reductions, hydrodimerisations, etc. However, suitable conditions and solvent systems for these types of processes are required.

There has been considerable interest in electrochemical processes at static triple-phase boundary systems including droplet[15,16] or micro-droplet deposits,[17] porous host electrodes for optimised triple-phase boundary zones,[18,19] microwire-based electrodes[20] and micro-droplet arrays on lithographically modified electrode surfaces.[21] Dynamic triple-phase boundary processes have recently been demonstrated for a two-phase flow with *N*-octyl-2-pyrrolidone (NOP) and aqueous electrolyte in contact with a gold electrode.[13] A quantitative expression for electrochemical processes under two-phase flow conditions was proposed, and the problem of 'undercutting' of the organic phase under the aqueous phase highlighted. Gold electrodes are of limited use in electrosynthesis applications, and indeed they are

* *Correspondence to: F. Marken, Department of Chemistry, University of Bath, Claverton Down, Bath BA2 7AY, UK.*
E-mail: f.marken@bath.ac.uk

a *S. M. MacDonald, J. D. Watkins, S. D. Bull, I. R. Davies, F. Marken*
Department of Chemistry, University of Bath, Claverton Down, Bath BA2 7AY, UK

b *Y. Gu, K. Yunus, A. C. Fisher*
Department of Chemical Engineering, University of Cambridge, New Museums Site, Pembroke Street, Cambridge CB2 3RA, UK

c *P. C. B. Page, Y. Chan*
School of Chemical Sciences & Pharmacy, University of East Anglia, Norwich, Norfolk NR4 7TJ, UK

d *C. Elliott*
Department of Chemistry, Loughborough University, Loughborough, Leicestershire LE11 3TU, UK

Journal of Physical Organic Chemistry

easily destroyed under anodic polarisation or in aggressive media. A much more versatile and more durable electrode material is boron-doped diamond (BDD).[22,23] We have recently demonstrated the use of BDD electrodes for the electrochemical formation of peroxocarbonate and peroxosulfate reagents in a clean catalytic two-phase epoxidation process employing an acetonitrile–water (electrolyte) reaction mixture.[24] We therefore consider acetonitrile–aqueous two-phase systems as highly interesting and important reaction media for two-phase electrochemistry. In this report, a novel two-phase flow system with a polycrystalline BDD electrode (highly polished to ensure laminar flow) is characterised and demonstrated for triple-phase boundary processes for two contrasting solvent systems: (i) NOP–aqueous and (ii) acetonitrile–aqueous.

When embedding electrodes into microfluidic devices, different configurations can be considered. Figure 1A shows a design in which 'pre-electrolysis' is applied and the aqueous phase is oxidised (e.g. to form ozone, bromine, peroxocarbonate, etc.) immediately before contact with the organic reactant phase.

In contrast to the pre-electrolysis configuration, in Fig. 1B the configuration for triple-phase boundary processes is presented. Here, both aqueous and organic phase are simultaneously in contact with the working electrode. The electrochemically active reagent is present in the organic phase and only a thin reaction zone (close to the triple-phase boundary zone in the centre) is active during the electrochemical reaction. The high electrical resistance within the organic phase restricts the reaction zone. Both configurations, Fig. 1A and 1B, are suitable for 'clean' electrosynthesis without intentionally including electrolyte in the organic phase. However, the investigation of the triple-phase boundary reaction zone in Fig. 1B is the main topic in this report. The physical parameters such as flow rate, viscosity and the diffusion coefficient of the reagent in the organic phase are investigated for their effect on the efficiency of triple-phase boundary electrosynthesis processes.

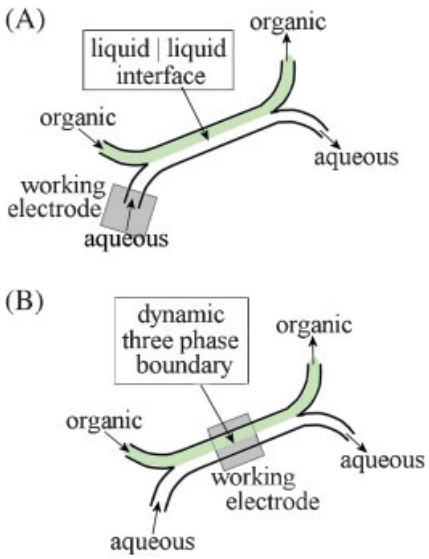

Figure 1. Schematic drawing of a dual flow microfluidic device for immiscible liquids. (A) 'Pre-electrolysis' design where a reactive reagent is formed immediately before the liquid–liquid interface is established. (B) 'Three-phase boundary' design where reagents are produced directly at the line interface between the two liquids

EXPERIMENTAL

Chemical reagents

Sodium perchlorate (99%, Aldrich), KCl, NaCl (both analytical grade, Aldrich), 5,10,15,20-tetraphenyl-21H,23H-porphine manganese (III) chloride (95%, Aldrich), acetonitrile (Fisons, for HPLC), NOP (>98.0%, Fluka), *n*-butylferrocene (98%, Alfa Aesar) and hexaammineruthenium(III)chloride (Alfa Aesar) were purchased and used without further purification. Argon (Pureshield, BOC, UK) was used to de-aerate solutions. Filtered and demineralised water was taken from an Elga water purification system with not less than 18 MOhm cm resistivity.

Instrumentation

Voltammetric measurements were conducted with a computer-controlled μ-Autolab III potentiostat system (Eco Chemie, The Netherlands) in staircase mode with a BDD working electrodes (Diafilm, 5 mm $\times$ 5 mm $\times$ 0.6 mm polished plates, Windsor Scientific, Slough, UK) and a platinum counter electrode situated downstream outside the double channel of the cell in the aqueous flow. A saturated calomel reference electrode (SCE, REF401, Radiometer) was placed upstream in the aqueous flow. This electrode was placed as close as possible to the cell inlet to optimise the potential control. Two synchronised Aladdin-1000 pumps (World Precision Instruments, USA) were used to control the flow rate of the two phases and to create the dynamic flow boundary running through the electrochemical cell. All experiments were conducted at $22 \pm 2^{\circ}$C.

Two-phase flow cell design and fabrication

The microchannel devices were fabricated in polydimethylsiloxane (PDMS) (Sylgard 184 Silicone Elastomer, Dow Corning), using standard soft lithographic techniques. The master mould was fabricated using SU-8 2100 (Microchem) photoresist using a previously published fabrication protocol.[25] The PDMS polymer was mixed with curing agent at the recommended ratio (10:1) and allowed to cure over period of 48 h at room temperature prior to use. All inlet and outlet channels were 500 μm wide and 250 μm high and the main channel expanded to twice the dimensions of 1 mm width and 250 μm height.

Another cured PDMS sheet containing a 5 mm $\times$ 5 mm inlaid BDD electrode was placed on top of PDMS microchannels to create a sealed environment using a Perspex clamp. The fabrication process of PDMS sheet with the integrated BDD electrode consists of two steps: (i) make a leading contact on back side of BDD electrode using conductive silver epoxy bonding, (ii) place the BDD electrode into a flat Petri dish and then casting the PDMS around the BDD electrode inside the Petri dish. After curing, removing the PDMS from the Petri dish revealed the BDD electrode embedded within the PDMS block (Fig. 2).

RESULTS AND DISCUSSION

Flow cell calibration with a single redox-active phase

Hydrodynamic voltammetry experiments conducted at electrodes embedded in a rectangular flow cell give rise to characteristic steady-state current responses with a mass transport-controlled limiting current as a function of the volume flow rate.[26] An equation which can be adapted to describe approximately this

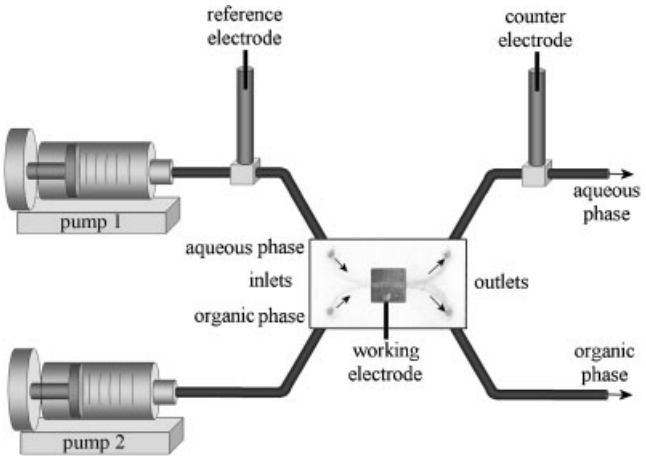

Figure 2. Schematic drawing of the two-phase flow cell system with two syringe pump feeds, external reference (aqueous flow, upstream) and counter (aqueous flow, downstream) electrode and two PDMS channels (500 μm wide, 500 μm high) joining into a combined channel (1000 μm wide, 500 high) in contact to the working electrode (5 mm × 5 mm BDD embedded in PDMS)

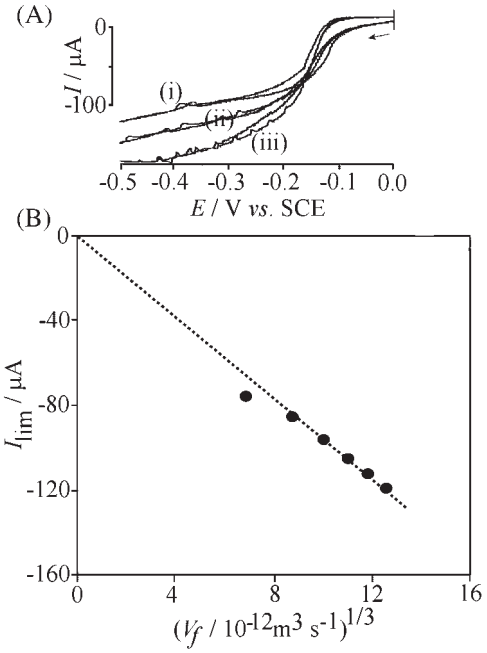

Figure 3. (A) Hydrodynamic cyclic voltammograms (5 mm length BDD electrode, scan rate 10 mVs^{-1}) for a solution of 10 mM $Ru(NH_3)_6^{3+}$ in aqueous 0.1 M KCl. The flow rates (for the combined channel) are (i) $3.33 \times 10^{-10}\ m^3s^{-1}$, (ii) $8.33 \times 10^{-10}\ m^3s^{-1}$ and (iii) $1.67 \times 10^{-9}\ m^3s^{-1}$. (B) Plot of the cathodic limiting current versus the cube root of flow rate. The dotted line represents the theoretical prediction based on Eqn 1 and assuming a channel height of $2h = 500\ \mu m$

limiting current predicts a cube root dependence of the mass transport-controlled limiting current, I_{lim}, on volume flow rate, V_f (Eqn 1):

$$I_{lim} = 0.925\, nFc\left(\frac{Dwx}{h}\right)^{2/3} V_f{}^{1/3} \quad (1)$$

In this equation I_{lim} is given by n, the number of electrons transferred per molecule diffusing to the electrode surface, F, the Faraday constant, c, the concentration of the reactive species in solution, D, the diffusion coefficient, h, the cell half height, w, the channel and electrode width and x, the electrode length. Strictly, this equation is valid only for electrodes with a width w smaller than the channel width. However, the error introduced by ignoring the boundary layer at the channel walls on the limiting current is small and can be ignored here.

A solution of 10 mM $Ru(NH_3)_6^{3+}$ in aqueous 0.1M KCl was employed to calibrate the cell dimensions. Figure 3A shows voltammograms obtained under flow conditions with both channels being employed for the aqueous flow. The mass transport-controlled limiting current was obtained as a function of flow rate, and a typical plot of the limiting current I_{lim} versus the cube root of flow rate is shown in Fig. 3B. The dotted line indicates the theoretical line based on Eqn 1, and employing $n = 1$, the diffusion coefficient,[27] $D(Ru(NH_3)_6^{3+}) = 0.9 \times 10^{-9}\ m^2s^{-1}$, the cell width $w = 1 \times 10^{-3}$ m, the half height $h = 0.25 \times 10^{-3}$ m and the electrode length $x = 5 \times 10^{-3}$ m. No adjustable parameters are required.

Flow cell processes with two-phase flow: I. Imaging and calibration of NOP–aqueous electrolyte flow

For two immiscible liquids flowing through the cell a dynamic phase boundary is produced, which crosses the BDD working electrode approximately in the centre. The exact position of the phase boundary is dependent on the flow conditions and the nature of the liquids. Here, the aqueous phase is in contact with either NOP or acetonitrile. The key physical properties of these liquids are summarised in Table 1.

In order to characterise the phase boundary during flow, MnTPPCl is employed as a green dye in the NOP phase, and microscopy images of the phase boundary are recorded as a function of flow conditions. Figure 4 shows typical images as well as a plot of the volume flow rate ratio $V_{f\,aqueous}/V_{f\,organic}$ versus the phase width ratio $\delta_{aqueous}/\delta_{organic}$.

From optical micrographs it is clear that the flow rate ratio $V_{faqueous}/V_{f\,organic}$ determines the position of the phase boundary. A higher rate of aqueous flow rate widens the area of the electrode in contact with the aqueous phase. The theoretical phase boundary position is also dependent on the liquid viscosities as shown in Eqn 2:

$$\frac{V_{f\,aqueous}}{V_{f\,organic}} = \alpha \times \frac{\delta_{aqueous}}{\delta_{organic}} \quad (2)$$

Table 1. Properties of solvents at 25°C

Solvent	Water	NOP	Acetonitrile
Viscosity (10^{-3} Pa s)	1.0	5.6	0.34
Density (g cm^{-3})	1.00	0.92	0.786
Molecular weight ($gmol^{-1}$)	18.02	197.32	41.05
Boiling point (°C)	100	170–172	81–82
Melting point (°C)	0	−25	−48

Journal of Physical Organic Chemistry

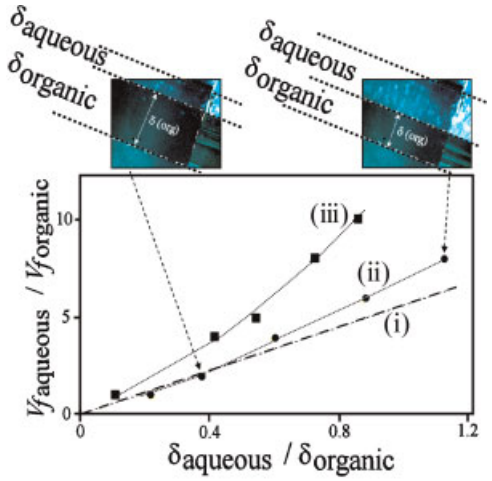

Figure 4. (Top) Optical micrographs of an NOP and aqueous 0.1 M KCl two-phase flow for two different volume flow rate ratios. (Bottom) A plot of the volume flow rate ratio $V_{f\ \mathrm{aqueous}}/V_{f\ \mathrm{organic}}$ versus the width of the aqueous phase divided by the width of the organic phase. The circular data points correspond to data for an organic flow rate of $8.33 \times 10^{-10}\,\mathrm{m^3 s^{-1}}$ (ii) and the square data points correspond to an organic flow rate of $1.67 \times 10^{-10}\,\mathrm{m^3 s^{-1}}$ (iii). The theoretical line (i) is based simply on the viscosity ratio according to Eqn 2 This figure is available in colour online at www.interscience.wiley.com/journal/poc

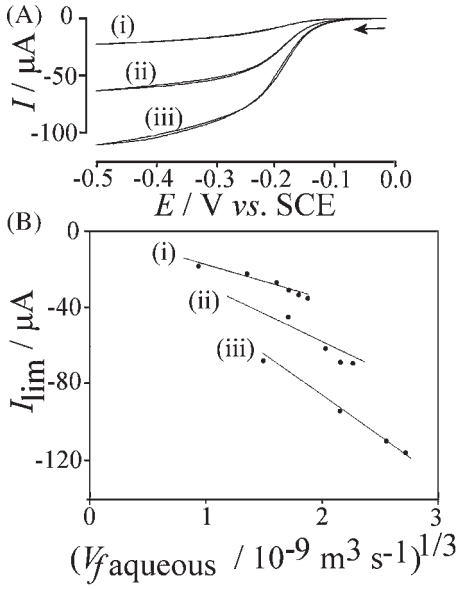

Figure 5. (A) Hydrodynamic cyclic voltammograms (scan rate 0.01 $\mathrm{Vs^{-1}}$, 5 mm length BDD electrode) for the reduction of 10 mM $Ru(NH_3)_6^{3+}$ in aqueous 0.5 M KCl flowing through the cell together with NOP. The ratio of $V_{f\ \mathrm{organic}}$ to $V_{f\ \mathrm{aqueous}}$ is (i) 1:5, (ii) 1:10, and (iii) 1:20. The theoretical line was calculated with Eqn 4 and with γ equal (i) 0.3, (ii) 0.4, and (iii) 0.5

In this equation $\alpha = \frac{\eta_{\mathrm{organic}}}{\eta_{\mathrm{aqueous}}}$ is the ratio of viscosities, which for the case of the NOP–water system[13] is ca. 5.6 (see Table 1). The theoretical line according to Eqn 2 is shown as line (i) in Fig. 4. A deviation of the experimental points from this line appears to increase as the flow rate is reduced. Optically, the organic phase can be seen to be drawn onto the electrode surface (not shown) thereby covering a wider section of the electrode surface. Surface tension effects are responsible for this behaviour.[13]

Next, redox processes in the presence of organic and aqueous flow were investigated. The parameter $\delta_{\mathrm{aqueous}}$ (the width of the aqueous phase during flow) may be derived from Eqn 2 (see Eqn 3) and then applied to Eqn 1 to give an estimate of the limiting current for a redox process within the aqueous phase (see Eqn 4):

$$\delta_{\mathrm{aqueous}} = \frac{w}{1+\alpha\frac{V_{f\,\mathrm{organic}}}{V_{f\,\mathrm{aqueous}}}} \tag{3}$$

$$I_{\mathrm{lim}} = 0.925\,nFc\left(\frac{\gamma Dwx}{h\left[1+\alpha\frac{V_{f\,\mathrm{organic}}}{V_{f\,\mathrm{aqueous}}}\right]}\right)^{2/3} V_{f\,\mathrm{aqueous}}{}^{1/3} \tag{4}$$

The constant γ has been included in this expression in order to express the effect of organic phase 'undercutting' the aqueous phase and therefore partially blocking the electrode.[13] Hydrodynamic voltammograms obtained for the reduction of $Ru(NH_3)_6^{3+}$ in aqueous 0.5 M KCl are shown in Fig. 5A. The analysis of the mass transport-controlled limiting currents as a function of both aqueous and organic flow rate is presented in Fig. 5B. A linear dependence of the limiting current on the cube root of aqueous flow rate is maintained (in agreement with Eqn 4 and suggesting convective diffusion), but the match between prediction based on Eqn 4 and experiment is poor (not shown). In all cases the currents are low consistent with the organic phase 'undercutting' the aqueous phase. This effect is most pronounced for slower flow rates (see Fig. 4B).

Flow cell processes with two-phase flow: II. Imaging and calibration of acetonitrile–aqueous electrolyte flow

Acetonitrile is a commonly used organic solvent and recently we have been able to achieve electrochemically driven catalytic epoxidation processes in a water–acetonitrile two-phase system.[24] Acetonitrile is water immiscible only in the presence of sufficiently high salt concentration in the aqueous phase. A remaining mutual miscibility between water and acetonitrile even in the presence of high salt concentrations exists. However, a stable liquid–liquid phase boundary is readily achieved and the diffusion controlled transfer of small quantities of acetonitrile into the aqueous phase can be minimised by maximising the flow speed. From data in Table 1 it can be seen that acetonitrile has a very low viscosity opposite to the value found for NOP. In principle, mixtures of acetonitrile and NOP could be employed to match the viscosity of the organic phase to the water viscosity, but in this study only the pure acetonitrile phase is investigated.

For acetonitrile–aqueous 1.5 M NaCl two-phase flow, optical observation allows the position of the phase boundary to be determined. The plot in Fig. 6 shows that, in contrast to data for NOP-aqueous two-phase flow, for all flow rates examined almost ideal behaviour is observed. No deviation from the viscosity-based prediction (see Eqn 2) occurs.

In electrochemical experiments under acetonitrile–aqueous electrolyte two-phase conditions, ideal behaviour of the triple-phase boundary is confirmed. Figure 7 shows typical plots of the mass transport-limited currents versus the cube root of aqueous flow rate.

The line indicates the expected limiting current based on Eqn 4 without any 'undercutting' effects. Good agreement is observed independent of the organic flow rate. Therefore the acetonitrile–aqueous electrolyte–BDD triple-phase boundary appears to provide ideal conditions for electrochemical processes.

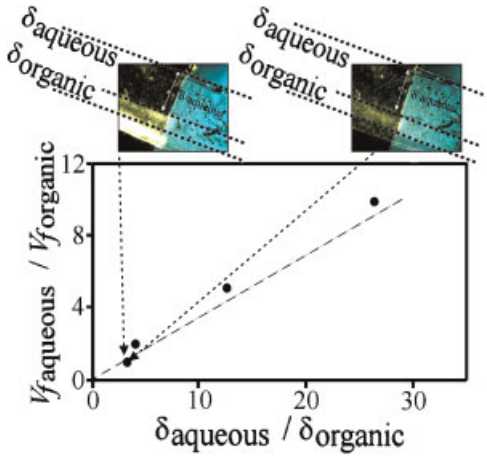

Figure 6. (Top) Optical observation of an acetonitrile and aqueous 1.5 M NaCl two-phase flow as a function of flow rate (left $V_{f\ \text{aqueous}} = V_{f\ \text{organic}} = 4.17 \times 10^{-10}\ \text{m}^3\text{s}^{-1}$, right $V_{f\ \text{aqueous}} = V_{f\ \text{organic}} = 2.0 \times 10^{-8}\ \text{m}^3\text{s}^{-1}$). (Bottom) A plot of the volume flow rate ratio $V_{f\ \text{aqueous}}/V_{f\ \text{organic}}$ versus the width of the aqueous phase divided by the width of the organic phase. The data points correspond to data at different flow rates. The theoretical line is based simply on the viscosity ratio according to Eqn 2 This figure is available in colour online at www.interscience.wiley. com/journal/poc

Flow cell processes with two-phase flow: III. Organic phase–aqueous electrolyte–solid electrode triple-phase boundary processes

With no intentionally added supporting electrolyte in the organic phase, redox processes in the organic phase are confined to a thin line along the triple-phase boundary. In order to explore and compare processes in NOP and in acetonitrile the *n*-butylferrocene redox system is employed. This redox system has been thoroughly studied for liquid–liquid electrochemical systems by Wadhawan *et al.*[28] In contrast to our earlier work,[13] here all experiments are conducted at a 5 mm × 5 mm BDD electrode.

Typical hydrodynamic voltammograms are shown in Fig. 8A for the oxidation of *n*-butylferrocene in an NOP phase in contact with an aqueous 1.5 M NaCl. In order to achieve conditions for a well-defined perchlorate anion transfer 0.1 M $NaClO_4$ is present in the aqueous phase.

The limiting current for the *n*-butylferrocene oxidation plotted versus the volume flow rate shows a decrease of current with higher flow rate. This is in contrast to bulk reactions, where an increase is always observed (see Eqns 1 and 4). This characteristic behaviour for hydrodynamic triple-phase boundary has been attributed to a growth in reaction zone with diffusion time[13] (vide infra). It is interesting to determine the conversion of *n*-butylferrocene (here defined as the ratio of mass transport limiting current and the total electrolysis current $nFcV_{f\ \text{organic}}$). The conversion remains very low, and only at an extremely low flow rate of $0.1 \times 10^{-9}\ \text{m}^3\text{s}^{-1}$ can a 10% conversion be achieved. For a bulk electrolysis process this is unsatisfactory. The plot of limiting

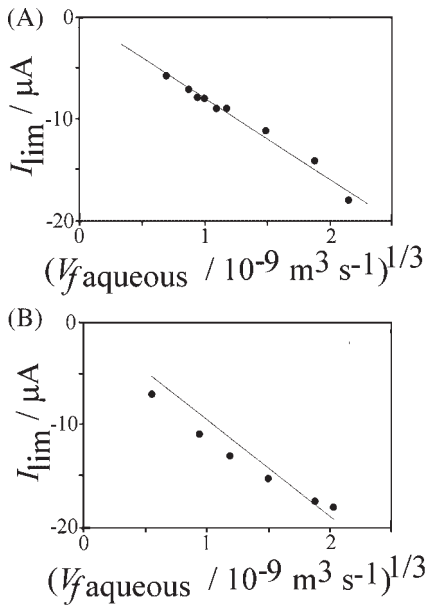

Figure 7. Plots of the mass transport-limited currents from hydrodynamic voltammograms for the reduction of 1 mM $Ru(NH_3)_6^{3+}$ at a 5 mm length BDD electrode in aqueous 1.5 M NaCl with simultaneous acetonitrile flow versus the cube root of aqueous flow. Data in (A) have been obtained for $V_{f\ \text{organic}}$: $V_{f\ \text{aqueous}}$ ratio of 1:1 data in and (B) have been obtained for $V_{f\ \text{organic}}$: $V_{f\ \text{aqueous}}$ ratio of 1:10. Lines indicate the theoretically predicted limiting current based on Eqn 4 with $\gamma = 1.0$

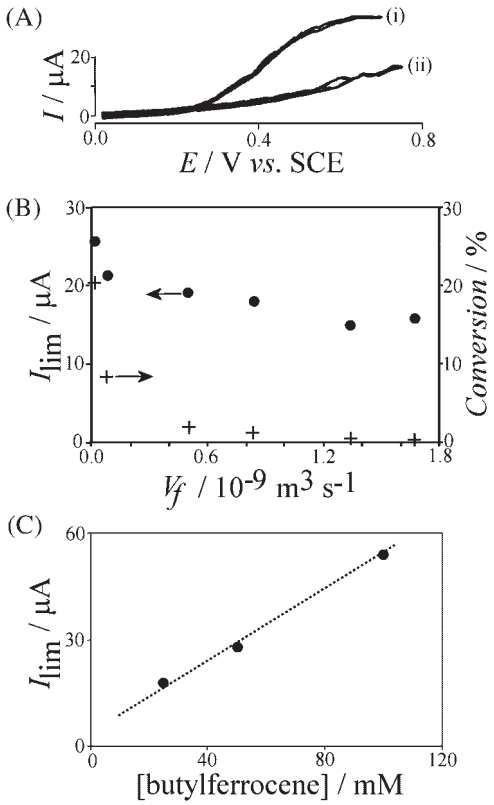

Figure 8. (A) Hydrodynamic cyclic voltammograms (scan rate 10 mVs^{-1}, $V_{f\ \text{organic}} = V_{f\ \text{aqueous}} = 8.33 \times 10^{-10}\ \text{m}^3\text{s}^{-1}$) for solutions of (i) 50 mM and (ii) 1 mM *n*-butylferrocene in NOP in the presence of aqueous 1.5 M NaCl and 0.1 M $NaClO_4$. (B) Plot of the mass transport limiting current obtained for the oxidation of 25 mM *n*-butylferrocene in NOP versus flow rate ($V_f = V_{f\ \text{organic}} = V_{f\ \text{aqueous}}$). (C) Plot of the mass transport limiting current for the oxidation of *n*-butylferrocene in acetonitrile versus concentration (aqueous phase 1.5 M NaCl and 0.1 M $NaClO_4$, $V_{f\ \text{organic}} = V_{f\ \text{aqueous}} = 1.67 \times 10^{-9}\ \text{m}^3\text{s}^{-1}$)

Journal of Physical Organic Chemistry

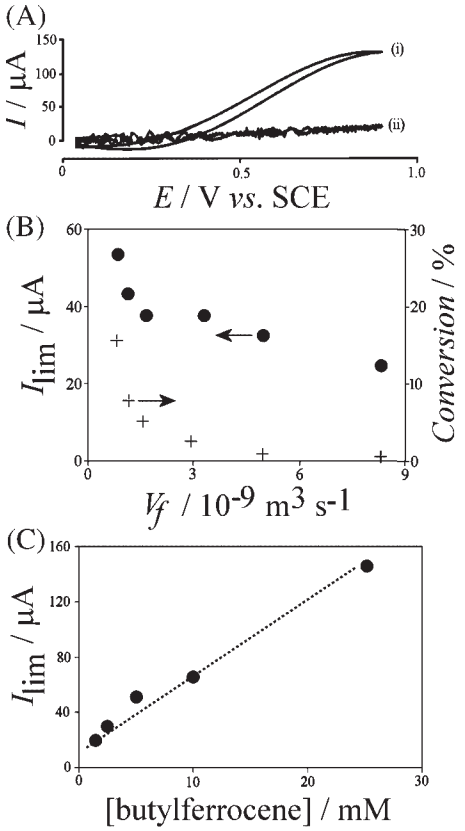

Figure 9. (A) Hydrodynamic cyclic voltammograms (scan rate 50 mVs^{-1}, $V_{f\ organic} = V_{f\ aqueous} = 1.67 \times 10^{-9}\,m^3s^{-1}$) for solutions of (i) 25 mM and (ii) 1 mM *n*-butylferrocene in acetonitrile in the presence of aqueous 1.5 M NaCl and 0.1 M $NaClO_4$. (B) Plot of the mass transport limiting current obtained for the oxidation of 6 mM *n*-butylferrocene in acetonitrile versus flow rate ($V_f = V_{f\ organic} = V_{f\ aqueous}$). (C) Plot of the mass transport limiting current for the oxidation of *n*-butylferrocene in acetonitrile versus concentration (aqueous phase 1.5 M NaCl and 0.1 M $NaClO_4$, $V_{f\ organic} = V_{f\ aqueous} = 1.67 \times 10^{-9}\,m^3s^{-1}$)

current versus *n*-butylferrocene concentration (see Fig. 8C) clearly suggests direct proportionality.

Next, experiments were conducted with *n*-butylferrocene dissolved in acetonitrile. Figure 9A shows typical hydrodynamic voltammograms. The plot of the mass transport-limited current versus flow rate (see Fig. 9B) again suggests a decrease of current at higher flow rates in good agreement with triple-phase boundary control. Limiting currents in acetonitrile are generally higher. A conversion of 10% is readily achieved at a flow rate an order of magnitude faster compared to that required in NOP. From the slope in the plot of the limiting current versus *n*-butylferrocene concentration (see Fig. 9C and Fig. 8C) it can be determined that the limiting currents are generally a factor of 12 higher in acetonitrile. The higher currents are predominantly due to the effect of viscosity (see Table 1, $\eta_{acetonitrile}/\eta_{water} = 16.5$) on the diffusion coefficient of the redox active *n*-butylferrocene. The effect of the triple-phase boundary geometry ('undercutting' in the NOP case) on the limiting current appears secondary.

It is interesting to compare the limiting current data for triple-phase boundary processes with those for line electrodes. An expression for the time-dependent limiting current at a line electrode in the absence of convection has been proposed by

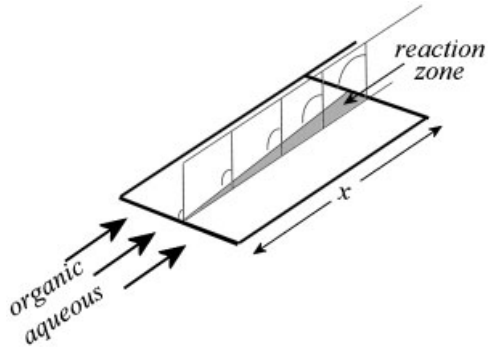

Figure 10. Schematic drawing of the reaction zone developing under hydrodynamic conditions at the three-phase boundary

Oldham,[29,30] and this equation is employed here with a factor ½ (see Eqn 5) in order to account for the fact that diffusion only occurs into the organic phase and not into the aqueous phase (see Fig. 10):

$$I(t) = \tfrac{1}{2} nFDcx\left(\sqrt{\tfrac{w_{TPB}}{\pi Dt}} + 1\right) \quad (5)$$

In this expression the time-dependent current is dependent on *n*, the number of electrons transferred per molecule diffusing to the electrode surface, *F*, the Faraday constant, *D*, the diffusion coefficient for *n*-butylferrocene[31] ($1.56 \times 10^{-9}\,m^2s^{-1}$), *c*, the bulk concentration of *n*-butylferrocene, *x*, the electrode length, *t*, the time and w_{TPB}, the width of the active electrode area at the triple-phase boundary. For conditions shown in Fig. 9B the steady-state current based on Eqn 5 (for $t \rightarrow \infty$) $I(\infty) = ½\ nFDCx = 2.2\,\mu A$, which is clearly lower compared to the experimental value of about 40 μA and therefore suggests non-steady-state conditions. The time for molecules to pass through the cell can be estimated (using Eqn 2) as $t = \frac{2hxw\alpha}{V_f(1+\alpha)}$ (with $\alpha = 0.34$ for acetonitrile, see Table 1) and in combination with Eqn 5 the approximate width of the triple-phase boundary $w_{TPB} \approx 1\,\mu m$ (for $V_f = 10^{-9}\,m^3s^{-1}$) is obtained (Eqn 6):

$$w_{TPB} \approx \frac{2\pi Dhxw}{V_f} \frac{\alpha}{1+\alpha}\left(\frac{2I}{nFDcx} - 1\right)^2 \quad (6)$$

It is very likely that the real timescale for molecules to pass through the cell is considerable higher due to slower flow close to the electrode surface, and therefore the active zone w_{TPB} is probably more extended. Also from Eqn 6 it appears that the volume flow rate is an important parameter causing a more extended active electrode zone for slower flow. Figure 10 shows a schematic diagram where the reaction zone is indicated as a wedge-shaped area that expands at slower flow rate. Only a more complex computer simulation approach will provide a more quantitative analysis in future. The two key results from this study are (i) the importance of viscosity as a parameter controlling conversion efficiency and (ii) the possibility of high conversion bulk electrolysis in acetonitrile–aqueous two-phase flow systems.

CONCLUSIONS

It has been shown that acetonitrile, a commonly employed low viscosity solvent in synthesis, is suitable for two-phase flow electrochemical reactor processes in the presence of aqueous 1.5 M NaCl. Well-defined two-phase flow is observed with a stable

triple-phase boundary electrolysis zone. When compared to *N*-octylpyrrolidone the lower viscosity considerably enhances mass transport and the rate of conversion. For acetonitrile the three-phase boundary zone is simple, and undercutting of the organic phase under the aqueous phase (which has been observed for NOP) remains insignificant. Experimental work addressing synthetically useful processes in a wider range of solvent systems and at more effective curved liquid–liquid phase boundaries is in progress.

Acknowledgements

SMM thanks the EPSRC for a studentship. This investigation has enjoyed the support of the EPSRC (Speculative Research Leading to Greener Chemical Technologies).

REFERENCES

[1] W. Ehrfeld, V. Hessel, H. Löwe, *Microreactors*, Wiley-VCH, Weinheim, **2000**. p. 166.
[2] P. He, P. Watts, F. Marken, S. J. Haswell, *Angew. Chem. Inter. Ed.* **2006**, *45*, 4146.
[3] D. Horii, T. Fuchigami, M. Atobe, *J. Am. Chem. Soc.* **2007**, *129*, 11692.
[4] J. Yoshida, S. Suga, A. Nagaki, *J. Synth. Org. Chem. Japan* **2005**, *63*, 511.
[5] C. A. Paddon, M. Atobe, T. Fuchigami, P. He, P. Watts, S. J. Haswell, G. J. Pritchard, S. D. Bull, F. Marken, *J. Appl. Electrochem.* **2006**, *36*, 617.
[6] S. Suga, M. Okajima, K. Fujiwara, J. Yoshida, *QSAR Comb. Sci.* **2005**, *24*, 728.
[7] S. Suga, *J. Synth. Org. Chem. Japan* **2006**, *64*, 1010.
[8] C. A. Paddon, G. J. Pritchard, T. Thiemann, F. Marken, *Electrochem. Commun.* **2002**, *4*, 825.
[9] T. Tajima, H. Kurihara, T. Fuchigami, *J. Am. Chem. Soc.* **2007**, *129*, 6680.
[10] T. Tajima, T. Fuchigami, *Angew. Chem. Inter. Ed.* **2005**, *44*, 4760.
[11] D. Horii, M. Atobe, T. Fuchigami, F. Marken, *J. Electrochem. Soc.* **2006**, *153*, D143.
[12] R. Horcajada, M. Okajima, S. Suga, J. Yoshida, *Chem. Commun.* **2005**, 1303.
[13] S. M. MacDonald, J. D. Watkins, Y. Gu, K. Yunus, A. C. Fisher, G. Shul, M. Opallo, F. Marken, *Electrochem. Commun.* **2007**, *9*, 2105.
[14] K. Yunus, C. B. Marks, A. C. Fisher, D. W. E. Allsopp, T. J. Ryan, R. A. W. Dryfe, S. S. Hill, E. P. L. Roberts, C. M. Brennan, *Electrochem. Commun.* **2002**, *4*, 579.
[15] F. Scholz, U. Schröder, R. Gulaboski, *Electrochemistry of Immobilized Particles and Droplets*, Springer, Berlin, **2005**.
[16] C. E. Banks, T. J. Davies, R. G. Evans, G. Hignett, A. J. Wain, N. S. Lawrence, J. D. Wadhawan, F. Marken, R. G. Compton, *Phys. Chem. Chem. Phys.* **2003**, *5*, 4093.
[17] F. Marken, R. D. Webster, S. D. Bull, S. G. Davies, *J. Electroanal. Chem.* **1997**, *437*, 209.
[18] M. A. Ghanem, F. Marken, *Electrochem. Commun.* **2005**, *7*, 1333.
[19] J. Niedziolka, K. Szot, F. Marken, M. Opallo, *Electroanalysis* **2007**, *19*, 155.
[20] E. Bak, M. Donten, Z. Stojek, F. Scholz, *Electrochem. Commun.* **2007**, *9*, 386.
[21] D. Rayner, N. Fietkau, I. Streeter, F. Marken, B. R. Buckley, P. C. B. Page, J. del Campo, R. Mas, F. X. Munoz, R. G. Compton, *J. Phys. Chem. C* **2007**, *111*, 9992.
[22] R. G. Compton, J. S. Foord, F. Marken, *Electroanalysis* **2003**, *15*, 1349.
[23] F. Marken, R. G. Compton, C. H. Goeting, J. S. Foord, S. D. Bull, S. G. Davies, *J. Solid State Electrochem.* **2001**, *5*, 88.
[24] P. C. B. Page, F. Marken, C. Williamson, Y. Chan, B. R. Buckley, D. Bethell, *Adv. Synth. Catal.* **2008**, *350*, 1149.
[25] S. M. Matthews, A. D. Elder, K. Yunus, C. F. Kaminski, C. M. Brennan, A. C. Fisher, *Anal. Chem.* **2007**, *79*, 4101.
[26] R. G. Compton, C. E. Banks, *Understanding Voltammetry*, World Scientific, Singapore, **2007**. p. 308.
[27] F Marken, JC Eklund, RG. Compton *J. Electroanal. Chem.* **1995**, *395*, 335.
[28] J. D. Wadhawan, R. G. Evans, R. G. Compton, *J. Electroanal. Chem.* **2002**, *533*, 71.
[29] J. A. Alden, R. G. Compton, R. A. W. Dryfe, *J. Electroanal. Chem.* **1995**, *397*, 11.
[30] K. B. Oldham, *J. Electroanal. Chem.* **1981**, *122*, 1.
[31] A. D. Clegg, N. V. Rees, O. V. Klymenko, B. A. Coles, R. G. Compton, *J. Electroanal. Chem.* **2005**, *580*, 78.